On- and off-resonance second-harmonic generation in GaAs microdisks

Paulina S. Kuo[1,*] and Glenn S. Solomon[1]

[1]*Joint Quantum Institute, National Institute of Standards & Technology and University of Maryland, Gaithersburg, MD 20899, USA*

[*]*pkuo@nist.gov*

Abstract: We present a theoretical description of on- and off-resonance, $\overline{4}$-quasi-phasematched, second-harmonic generation (SHG) in microdisks made of GaAs or other materials possessing $\overline{4}$ symmetry, such as GaP or ZnSe. The theory describes the interplay between quasi-phasematching (QPM) and the cavity-resonance conditions. For optimal conversion, all waves should be resonant with the microdisk and should satisfy the $\overline{4}$-QPM condition. We explore $\chi^{(2)}$ nonlinear mixing if one of the waves is not resonant with the microdisk cavity and calculate the second-harmonic conversion spectrum. We also describe perfectly destructive $\overline{4}$-QPM where both the fundamental and second-harmonic are on-resonance with the cavity but SHG is suppressed.

OCIS codes: (190.2620) Harmonic generation and mixing; (190.5970) Semiconductor nonlinear optics including MQW.

References and links

1. J. A. Armstrong, N. Bloembergen, J. Ducuing, and P. S. Pershan, "Interactions between light eaves in a nonlinear dielectric," Phys. Rev. **127**(6), 1918–1939 (1962).
2. M. M. Fejer, G. A. Magel, D. H. Jundt, and R. L. Byer, "Quasi-phase-matched second harmonic generation: tuning and tolerances," IEEE J. Quantum Electron. **28**(11), 2631–2654 (1992).
3. E. Lallier, M. Brevignon, and J. Lehoux, "Efficient second-harmonic generation of a CO_2 laser with a quasi-phase-matched GaAs crystal," Opt. Lett. **23**(19), 1511–1513 (1998).
4. S. Koh, T. Kondo, Y. Shiraki, and R. Ito, "GaAs/Ge/GaAs sublattice reversal epitaxy and its application to nonlinear optical devices," J. Cryst. Growth **227–228**(1-4), 183–192 (2001).
5. L. A. Eyres, P. J. Tourreau, T. J. Pinguet, C. B. Ebert, J. S. Harris, M. M. Fejer, L. Becouarn, B. Gerard, and E. Lallier, "All-epitaxial fabrication of thick, orientation-patterned GaAs films for nonlinear optical frequency conversion," Appl. Phys. Lett. **79**(7), 904–906 (2001).
6. R. Haidar, N. Forget, P. Kupecek, and E. Rosencher, "Fresnel phase matching for three-wave mixing in isotropic semiconductors," J. Opt. Soc. Am. B **21**, 1522–1534 (2004).
7. H. Komine, W. H. Long, Jr., J. W. Tully, and E. A. Stappaerts, "Quasi-phase-matched second-harmonic generation by use of a total-internal-reflection phase shift in gallium arsenide and zinc selenide plates," Opt. Lett. **23**(9), 661–663 (1998).
8. C. Simonneau, J. P. Debray, J. C. Harmand, P. Vidakovi, D. J. Lovering, and J. A. Levenson, "Second-harmonic generation in a doubly resonant semiconductor microcavity," Opt. Lett. **22**(23), 1775–1777 (1997).
9. Y. Dumeige and P. Féron, "Whispering-gallery-mode analysis of phase-matched doubly resonant second-harmonic generation," Phys. Rev. A **74**(6), 063804 (2006).
10. Z. Yang, P. Chak, A. D. Bristow, H. M. van Driel, R. Iyer, J. S. Aitchison, A. L. Smirl, and J. E. Sipe, "Enhanced second-harmonic generation in AlGaAs microring resonators," Opt. Lett. **32**(7), 826–828 (2007).
11. P. S. Kuo, W. Fang, and G. S. Solomon, "4-quasi-phase-matched interactions in GaAs microdisk cavities," Opt. Lett. **34**(22), 3580–3582 (2009).
12. R. T. Horn and G. Weihs, "Directional Quasi-Phase Matching in Curved Waveguides," http://arXiv.org/abs/1008.2190v1.
13. W. J. Kozlovsky, C. D. Nabors, and R. L. Byer, "Efficient second harmonic generation of a diode-laser-pumped CW Nd:YAG laser using monolithic MgO:$LiNbO_3$ external resonant cavities," IEEE J. Quantum Electron. **24**(6), 913–919 (1988).
14. Z. Yang and J. E. Sipe, "Generating entangled photons via enhanced spontaneous parametric downconversion in AlGaAs microring resonators," Opt. Lett. **32**(22), 3296–3298 (2007).
15. V. S. Ilchenko, A. A. Savchenkov, A. B. Matsko, and L. Maleki, "Nonlinear optics and crystalline whispering gallery mode cavities," Phys. Rev. Lett. **92**(4), 043903 (2004).

#149422 - $15.00 USD Received 20 Jun 2011; revised 25 Jul 2011; accepted 25 Jul 2011; published 15 Aug 2011

16. J. U. Fürst, D. V. Strekalov, D. Elser, M. Lassen, U. L. Andersen, C. Marquardt, and G. Leuchs, "Naturally phase-matched second-harmonic generation in a whispering-gallery-mode resonator," Phys. Rev. Lett. **104**(15), 153901 (2010).
17. K. Rivoire, Z. Lin, F. Hatami, W. T. Masselink, and J. Vucković, "Second harmonic generation in gallium phosphide photonic crystal nanocavities with ultralow continuous wave pump power," Opt. Express **17**(25), 22609–22615 (2009).
18. A. Rodriguez, M. Soljačić, J. D. Joannopoulos, and S. G. Johnson, "$\chi^{((2))}$ and $\chi^{((3))}$ harmonic generation at a critical power in inhomogeneous doubly resonant cavities," Opt. Express **15**(12), 7303–7318 (2007).
19. A. Yariv, "Universal relations for coupling of optical power between microresonators and dielectric waveguides," Electron. Lett. **36**(4), 321–322 (2000).
20. T. Skauli, P. S. Kuo, K. L. Vodopyanov, T. J. Pinguet, O. Levi, L. A. Eyres, J. S. Harris, M. M. Fejer, B. Gerard, L. Becouarn, and E. Lallier, "Improved dispersion relations for GaAs and applications to nonlinear optics," J. Appl. Phys. **94**(10), 6447–6455 (2003).
21. J. U. Nöckel, A. D. Stone, and R. K. Chang, "*Q* spoiling and directionality in deformed ring cavities," Opt. Lett. **19**(21), 1693–1695 (1994).
22. C. Gmachl, F. Capasso, E. E. Narimanov, J. U. Nockel, A. D. Stone, J. Faist, D. L. Sivco, and A. Y. Cho, "High-power directional emission from microlasers with chaotic resonators," Science **280**(5369), 1556–1564 (1998).
23. Y. Dumeige, "Quasi-phase-matching and second-harmonic generation enhancement in a semiconductor microresonator array using slow-light effects," Phys. Rev. A **83**(4), 045802 (2011).
24. A. Andronico, I. Favero, and G. Leo, "Difference frequency generation in GaAs microdisks," Opt. Lett. **33**(18), 2026–2028 (2008).
25. M. Borselli, T. J. Johnson, and O. Painter, "Beyond the Rayleigh scattering limit in high-*Q* silicon microdisks: theory and experiment," Opt. Express **13**(5), 1515–1530 (2005).
26. C. R. Pollock, *Fundamentals of Optoelectronics* (Irwin, 1995).
27. A. Yariv, "Coupled-mode theory for guided-wave optics," IEEE J. Quantum Electron. **9**(9), 919–933 (1973).
28. K. R. Hiremath, M. Hammer, R. Stoffer, L. Prkna, and J. Čtyroký, "Analytic approach to dielectric optical bent slab waveguides," Opt. Quantum Electron. **37**(1-3), 37–61 (2005).
29. H. A. Haus, *Waves and Fields in Optoelectronics* (Prentice-Hall, 1984).
30. M. Borselli, Ph.D. thesis (California Institute of Technology, 2006).
31. T. Skauli, K. L. Vodopyanov, T. J. Pinguet, A. Schober, O. Levi, L. A. Eyres, M. M. Fejer, J. S. Harris, B. Gerard, L. Becouarn, E. Lallier, and G. Arisholm, "Measurement of the nonlinear coefficient of orientation-patterned GaAs and demonstration of highly efficient second-harmonic generation," Opt. Lett. **27**(8), 628–630 (2002).

1. Introduction

GaAs and other zincblende-structured crystals such as GaP and ZnSe are attractive nonlinear optical materials because of their large nonlinear coefficients and broad transmission ranges. These materials cannot be birefringently phasematched so other means of phasematching are required to achieve efficient nonlinear frequency conversion. Efficient conversion has been demonstrated in GaAs by quasi-phasematching (QPM) [1,2] using periodic domain inversions [3–5] and by Fresnel phasematching [6,7]. QPM in GaAs has also been shown using phase-shifting mirrors [8].

Recently, $\bar{4}$-quasi-phasematching ($\bar{4}$-QPM) in GaAs microdisks and microrings has been proposed [9–11]. $\bar{4}$-QPM allows efficient $\chi^{(2)}$ nonlinear optical mixing of the whispering-gallery modes of a GaAs microdisk without using external domain inversions. The $\bar{4}3m$ symmetry of zincblende semiconductors (such as GaAs, GaP and ZnSe) means that a 90° rotation about the <001> axis is equivalent to a domain inversion (see Figs. 1a and 1b). As waves propagate around a <001>-surface-normal microdisk, their crystal environment effectively experiences four 90° rotations, which is equivalent to four domain inversions due to the $\bar{4}$-symmetry (Fig. 1c). The nonlinear tensor for $\bar{4}3m$ materials dictates that one of the three interacting waves in the <001>-surface-normal microdisk must have TM polarization (electric field orthogonal to the disk) while the other two have TE polarization (electric field in the plane of the disk). The QPM effect can be seen by considering the interaction of the fields with the nonlinear tensor [9], as described for $\bar{4}3m$ crystals in Appendix A. In additional to microdisks and microrings, $\bar{4}$-QPM can be obtained in other "bent" geometries such as square-shaped resonators [11] and curved waveguides [12]. $\bar{4}$-QPM is also available in other crystals with $\bar{4}$-symmetry such as those of the $\bar{4}2m$ (KH_2PO_4, chalcopyrites, etc.), and $\bar{4}$ crystal classes [11].

#149422 - $15.00 USD Received 20 Jun 2011; revised 25 Jul 2011; accepted 25 Jul 2011; published 15 Aug 2011

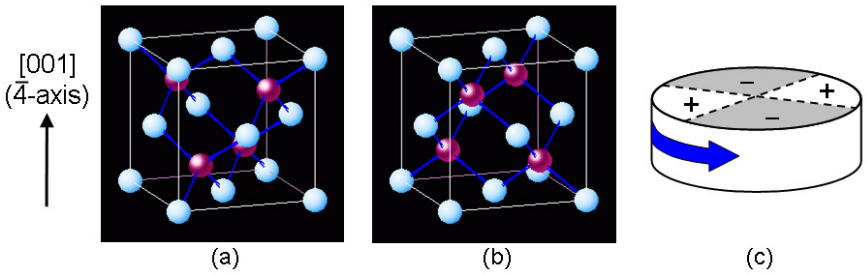

Fig. 1. Two views of the zincblende crystal structure with (a) inverted relative to (b). $\bar{4}$ symmetry means that a 90° rotation combined with a crystal inversion reproduces the original crystal. Equivalently, a 90° rotation about the $\bar{4}$ axis is the same as a crystal inversion. (c) Waves propagating around a <001>-normal GaAs microdisk effectively experience four 90° rotations and hence, four domain inversions.

The nonlinear conversion efficiency is also increased by the presence of the resonant cavity. External cavities have been used to enhance second-harmonic generation (SHG) in bulk crystals [13]. Resonantly enhanced nonlinear mixing can enable efficient optical-frequency conversion in small volumes, which would be of interest for miniature integrated sources and generation of entangled photons [14]. Cavity-enhanced SHG has been demonstrated in microcavities including $LiNbO_3$ whispering-gallery-mode resonators [15,16] and GaP photonic-crystal cavities [17]. In nonlinear microcavities where all the interacting waves are on-resonance, 100% conversion can be obtained theoretically with milliwatt-level pumping [18].

In this paper, we explore the interplay between cavity resonances and $\bar{4}$-QPM in enhancing nonlinear-conversion efficiency in a GaAs microdisk. We describe on- and off-resonance nonlinear-optical conversion. As an example, we consider SHG in a GaAs microdisk, but our results can be extended to three-frequency processes such as sum- and difference-frequency generation, and to other $\bar{4}$-symmetry materials. We present a theoretical analysis in Section 2 of $\bar{4}$-QPM in a traveling wave resonator. To maximize conversion, both fundamental and second-harmonic waves should be resonant with the microdisk and the $\bar{4}$-QPM condition should be satisfied. We investigate nonlinear conversion if one of the waves is not resonant with the microdisk cavity and calculate the conversion in these cases. We explore the effects of varying microdisk radius and temperature on the SH conversion spectrum in Section 3, which is important for experimental realization of SHG in a GaAs microdisk. In Section 4, we discuss interpretations of our results including analogies to Fresnel phasematching. We also describe perfectly destructive $\bar{4}$-quasi-phasematching where both the fundamental and second-harmonic waves are on-resonance but SHG is suppressed.

2. SHG conversion efficiency based on generalized waveguide-microresonator coupling theory

In an air-clad GaAs microdisk with $\hat{z}$ surface-normal, SHG occurs for a TE-polarized fundamental (electric field in the plane of the disk, with magnetic field, H_z^f) and a TM-polarized second-harmonic (SH) (electric field orthogonal to the disk, E_z^{SH}). With coordinates sketched in Fig. 2a, the fields can be represented by

#149422 - $15.00 USD Received 20 Jun 2011; revised 25 Jul 2011; accepted 25 Jul 2011; published 15 Aug 2011

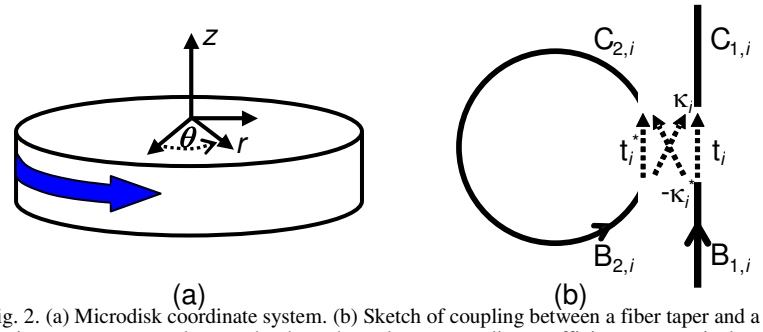

Fig. 2. (a) Microdisk coordinate system. (b) Sketch of coupling between a fiber taper and a disk or ring resonator. t_i and κ_i are the through- and cross-coupling coefficients, respectively; and i represents f or SH.

$$H_z^f = A_f(\theta,t)\Psi_f(r,z)e^{i(\omega_f t - m_f\theta)}$$
$$E_z^{SH} = A_{SH}(\theta,t)\Psi_{SH}(r,z)e^{i(\omega_{SH} t - m_{SH}\theta)}, \quad (1)$$

where $A_i(\theta,t)$ is the slowly varying amplitude at frequency ω_i (the index i refers to the fundamental, f, or the second-harmonic, SH). In this section, $A_i(\theta,t)$ is normalized so that $|A_i(\theta,t)|^2$ = power. $\Psi_i(r, z)$ is the mode profile, and m_i is the azimuthal number of the mode, which is an integer for a resonant mode. The $\exp(-im_i\theta)$ factors describe the phase accumulated by the waves as they propagate around the disk, analogous to $\exp(-ik_i\ell)$ terms found in linear propagation geometries. The change in the SH amplitude due to nonlinear mixing in the GaAs microdisk is described by [9,11]

$$\frac{\partial A_{SH}}{\partial\theta} = A_f{}^2\left(K_+ e^{i(\Delta m+2)\theta} + K_- e^{i(\Delta m-2)\theta}\right), \quad (2)$$

where $\Delta m = m_{SH} - 2m_f$, and K_+ and K_- are the SHG coefficients. Details of the fields inside the microdisk and the derivation of Eq. (2) are discussed in Appendix A. If we assume the fundamental is undepleted (A_f is constant), integrating Eq. (2) from $\theta = 0$ to 2π yields

$$A_{SH}(2\pi) - A_{SH}(0) = A_f{}^2\tilde{K}, \quad (3)$$

where

$$\tilde{K} = 2\pi\left(K_+ e^{i\pi(\Delta m+2)}\,\mathrm{sinc}[(\Delta m+2)\pi] + K_- e^{i\pi(\Delta m-2)}\,\mathrm{sinc}[(\Delta m-2)\pi]\right), \quad (4)$$

and $\mathrm{sinc}(x) = \sin(x)/x$. Equation (3) describes the change in the amplitude of the second-harmonic wave due to SHG and does not include loss.

Let us consider coupling of the microdisk to a waveguide (Fig. 2b). $B_{n,i}$ and $C_{n,i}$ are the complex mode amplitudes normalized so that $|B_{n,i}|^2$, $|C_{n,i}|^2$ = power. We note that $B_{n,i}$ and $C_{n,i}$ differ from the slowly varying amplitudes $A_i(\theta, t)$ by phase terms. Following Ref [19], coupling between the resonator and waveguide (in the absence of reflections) is described by

$$\begin{bmatrix} C_{1,i} \\ C_{2,i} \end{bmatrix} = \begin{bmatrix} t_i & \kappa_i \\ -\kappa_i^* & t_i^* \end{bmatrix}\begin{bmatrix} B_{1,i} \\ B_{2,i} \end{bmatrix}. \quad (5)$$

The coupler is taken to be lossless so that $|\kappa_i|^2 + |t_i|^2 = 1$.

Propagation of the fundamental around the ring produces loss, α_f, and phase shift, ϕ_f,

$$B_{2,f} = \alpha_f \exp(i\phi_f)C_{2,f}. \quad (6)$$

#149422 - $15.00 USD Received 20 Jun 2011; revised 25 Jul 2011; accepted 25 Jul 2011; published 15 Aug 2011

At the SH wave, there is loss, phase shift and SHG gain. Equation (3) may be written as

$$\frac{B_{2,SH}}{\alpha_{SH}\exp(i\phi_{SH})} - C_{2,SH} = \left|C_{2,f}\right|^2 \tilde{K}. \tag{7}$$

We assume the amplitude of the fundamental wave is constant ($A_f^2 \approx |C_{2,f}|^2 \approx |B_{2,f}|^2$).

The quantity m_i plays a role analogous to the wavevector k_i in linear propagation geometries. Both describe the rate of phase accumulation due to propagation and, hence, the effective propagation constant inside the medium. However, m_i is only well-defined at cavity-resonance wavelengths. Inside the microdisk, it is reasonable to ask what the effective propagation constant is at a wavelength that does not fall at a cavity resonance. We can estimate this effective propagation constant by linearly interpolating between resonances of the same spatial-mode family and constructing a function $m_i'(\lambda_i)$. This continuous function describes the effective dispersion inside the microdisk. The phase shift from one round trip in the disk is

$$\phi_i = -2\pi m_i', \tag{8}$$

and the phase mismatch per round trip accumulated between the fundamental and SH waves is

$$-2\pi\Delta m' = \phi_{SH} - 2\phi_f. \tag{9}$$

We can extend the description of SHG in a microdisk to include cases where the fundamental and/or SH waves are not resonant with the cavity by replacing Δm by $\Delta m'$ in Eqs. (2) – (4).

Using Eqs. (5) and (6), the circulating fundamental power is [19]

$$\left|B_{2,f}\right|^2 = \frac{\alpha_f{}^2\left(1-|t_f|^2\right)}{1+\alpha_f{}^2|t_f|^2-2\alpha_f|t_f|\cos(\psi_f+\phi_f)}\left|B_{1,f}\right|^2, \tag{10}$$

and the transmitted power is

$$\left|C_{1,f}\right|^2 = \frac{\alpha_f{}^2+|t_f|^2-2\alpha_f|t_f|\cos(\psi_f+\phi_f)}{1+\alpha_f{}^2|t_f|^2-2\alpha_f|t_f|\cos(\psi_f+\phi_f)}\left|B_{1,f}\right|^2, \tag{11}$$

where

$$t_i = \left|t_i\right|\exp(-i\psi_i). \tag{12}$$

We note that Eqs. (10) and (11) also describe the "passive" behavior of the resonator at the second-harmonic wavelength when the *f* subscripts are replaced by *SH*.

For SHG in the microresonator, there is no incoming wave at the second-harmonic ($B_{1,SH} = 0$) so that Eq. (5) becomes

$$\begin{aligned} C_{1,SH} &= \kappa_{SH} B_{2,SH} \\ C_{2,SH} &= t_{SH}^* B_{2,SH}. \end{aligned} \tag{13}$$

If we assume that the amplitude of the fundamental wave is unchanged (that is, $\alpha_f \approx 1$ and $|C_{2,f}|^2 \approx |B_{2,f}|^2$), it follows from Eqs. (7) and (13) that the circulating second-harmonic power is

#149422 - $15.00 USD Received 20 Jun 2011; revised 25 Jul 2011; accepted 25 Jul 2011; published 15 Aug 2011

$$\left|B_{2,SH}\right|^2 = \left|B_{2,f}\right|^4 \frac{\left|\tilde{K}\right|^2 {\alpha_{SH}}^2}{1+{\alpha_{SH}}^2 |t_{SH}|^2 - 2\alpha_{SH}|t_{SH}|\cos(\psi_{SH}+\phi_{SH})}$$
$$= \left|B_{1,f}\right|^4 \frac{\left|\tilde{K}\right|^2 {\alpha_{SH}}^2}{1+{\alpha_{SH}}^2 |t_{SH}|^2 - 2\alpha_{SH}|t_{SH}|\cos(\psi_{SH}+\phi_{SH})} \quad (14)$$
$$\times \left(\frac{{\alpha_f}^2 (1-|t_f|^2)}{1+{\alpha_f}^2 |t_f|^2 - 2\alpha_f |t_f| \cos(\psi_f+\phi_f)} \right)^2 .$$

The transmitted SH power is

$$\left|C_{1,SH}\right|^2 = \left|B_{2,SH}\right|^2 (1-|t_{SH}|^2). \quad (15)$$

The parameters α_i and t_i are related to the quality factors of the resonator. From Ref [19], the linewidths of the resonances are calculated by considering the shift in phase ϕ_i where the circulating power (Eq. (10)) is half of its peak value. The finesse at wave i, F_i, is the ratio between the phase shift between adjacent resonances, 2π, and the full-width at half maximum (FWHM) of the resonance. The finesse is also equal to the free spectral range (FSR) divided by the FWHM of the resonance. For a high-finesse resonator where $\alpha_i, |t_i| \approx 1$, the finesse is

$$F_i = \frac{2\pi}{2\Delta(\psi_i+\phi_i)} = \pi \frac{\sqrt{\alpha_i |t_i|}}{1-\alpha_i |t_i|} = \frac{\delta\omega_{FSR}}{\Delta\omega_{FWHM}}. \quad (16)$$

The quality factor, Q_i, is ratio between the resonance frequency, ω_0, and the linewidth, $\Delta\omega_{FWHM}$, and can be calculate from the finesse using

$$Q_i = \frac{\omega_0}{\Delta\omega_{FWHM}} = F_i \frac{\omega_0}{\delta\omega_{FSR}} = \pi \frac{\sqrt{\alpha_i |t_i|}}{1-\alpha_i |t_i|} \frac{\omega_0}{\delta\omega_{FSR}}. \quad (17)$$

The total (Q_i), intrinsic (Q_i^0) and coupling (Q_i^c) quality factors are related by

$$\frac{1}{Q_i} = \frac{1}{Q_i^0} + \frac{1}{Q_i^c}, \quad (18)$$

where

$$Q_i^0 = \pi \frac{\sqrt{\alpha_i}}{1-\alpha_i} \frac{c}{\lambda_i \delta f_{i,FSR}} \qquad Q_i^c = \pi \frac{\sqrt{|t_i|}}{1-|t_i|} \frac{c}{\lambda_i \delta f_{i,FSR}}. \quad (19)$$

c is the speed of light, λ_i is the wavelength, and $\delta f_{i,FSR}$ is FSR in frequency units of wave i.

3. On- and off-resonance second-harmonic generation in a GaAs microdisk

Using Eqs. (14) and (15), we can understand SHG in a microdisk for the cases when both the fundamental and SH are resonant with the microdisk cavity, and for the cases when one or more of the waves is not resonant. We consider SHG with $\lambda_f \approx 2$ μm in 161-nm thick GaAs microdisks where both fundamental and SH modes are the lowest-order vertical and lowest-order radial modes. The disk thickness is chosen so that doubly resonant, quasi-phasematched SHG can be supported with disk radii near 2.6 μm. Throughout this section, we take the incident fundamental power (in the fiber waveguide) as $P_f^{in} = \left|B_{1,f}\right|^2 = 1$ mW and $Q_f^0 = Q_f^c = Q_{SH}^0 = Q_{SH}^c = 10000$, which corresponds to linewidths $\Delta\lambda_f = 2\Delta\lambda_{SH} = 0.4$ nm. We also

#149422 - $15.00 USD Received 20 Jun 2011; revised 25 Jul 2011; accepted 25 Jul 2011; published 15 Aug 2011

assume the phase shifts from the coupler are $\psi_f = \psi_{SH} = 0$ (the main effects of non-zero coupler phase shifts are small wavelength shifts in the resonance locations). Values for K_+ and K_- are given in Table 1 of Appendix B.

A GaAs disk with radius R = 2.609 μm has both the fundamental and SH waves on-resonance at $\lambda_f = 2\lambda_{SH}$ = 1998.7 nm with fundamental wave (m_f = 13) TE-polarized and the SH wave (m_{SH} = 28) TM-polarized (satisfying $m_{SH} - 2m_f = 2$). We used finite-element modeling software and GaAs dispersion data [20] to calculate resonance wavelengths for various values of m_f and m_{SH}, and linearly interpolated between resonances to calculate $m_i'(\lambda)$ and the phase shifts, ϕ_i (Eq. (8)). Figure 3 shows the SH conversion efficiency, $\eta = |C_{1,SH}|^2 / |B_{1,f}|^2$, for this microdisk.

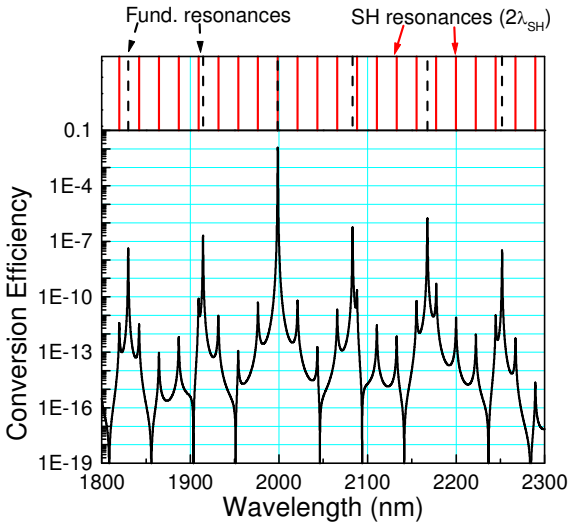

Fig. 3. SH conversion efficiency for various pumping wavelengths in a GaAs microdisk (R = 2.609 μm, h = 161nm) that supports doubly resonant SHG at $\lambda_f = 2\lambda_{SH}$ = 1998.7 nm (where m_f = 13, m_{SH} = 28, Δm = 2). The maximum conversion efficiency is η = 1.2% for 1 mW of incident fundamental power. The top inset shows locations of the fundamental and SH ($2\lambda_{SH}$) cavity resonances.

A maximum conversion of η = 1.2% is obtained at a pumping wavelength of 1998.7 nm. At this wavelength, both the fundamental and SH waves are resonant with the microdisk and $\Delta m = m_{SH} - 2m_f = 2$. Figure 3 also shows the SH conversion efficiency at other wavelengths that do not necessarily correspond to cavity resonances. When the fundamental is on-resonance but the SH is not, there is a local maximum in η, but its value is more than four orders of magnitude smaller than the maximum conversion found at 1998.7 nm. There are also local maxima when only the SH is on-resonance and the fundamental is not, but these peaks are even weaker than the fundamental-only peaks. The difference in relative peak sizes confirms that resonance-enhancement at the fundamental wave is a larger contributor to increased SHG than resonance-enhancement at the SH wave, which can also be seen in the expression for SHG calculated by coupled-mode theory (Eq. (62) in Appendix B) where P_{SH}^{out} is roughly proportional to $Q_{SH}^c (Q_f^c)^2$.

Another feature of Fig. 3 are the sharp dips in the SH conversion. These dips correspond to wavelengths where $\Delta m' = 0,\ \pm 1, \pm 3$, etc., and there is perfectly destructive $\overline{4}$-QPM. These wavelengths need not correspond to cavity resonances; for instance, $\Delta m' = 0$ occurs at λ_f = 2093.7 nm in Fig. 3 where m_f' = 11.87 and m_{SH}' = 23.75. SHG is suppressed at these wavelengths in the same way that nonlinear conversion is suppressed in even-order QPM gratings having 50% duty cycle [2].

#149422 - $15.00 USD Received 20 Jun 2011; revised 25 Jul 2011; accepted 25 Jul 2011; published 15 Aug 2011

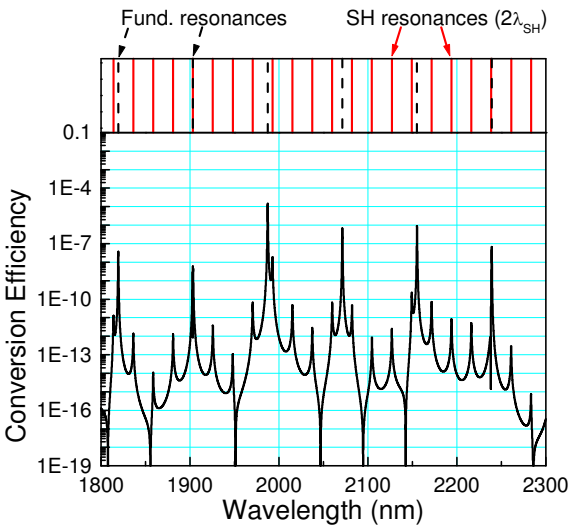

Fig. 4. SH conversion efficiency for different pumping wavelengths in a GaAs microdisk (R = 2.587 μm, h = 161nm). Near 1990 nm where $\Delta m' \approx 2$, the fundamental and SH resonances do not overlap and are separated by $\lambda_f - 2\lambda_{SH} = -5.4$ nm. The maximum SH conversion occurs at a pumping wavelength of 1987.4 nm with $\eta = 1.4 \times 10^{-3\%}$ (P_f^{in} = 1 mW). The top inset shows locations of the fundamental and SH ($2\lambda_{SH}$) cavity resonances.

Figure 4 plots the SH conversion for a slightly smaller GaAs microdisk (R = 2.587 μm, h = 161 nm) where the fundamental and SH resonances near 1990 nm do not overlap. For this disk, the m_f = 13 fundamental resonance occurs at λ_f = 1987.4 nm and the m_{SH} = 28 SH resonance occurs at $2\lambda_{SH}$ = 1992.8 nm such that $|\lambda_f - 2\lambda_{SH}| = 5.4$ nm. A maximum conversion of $\eta = 1.4\times10^{-3}\%$ is obtained at a pumping wavelength of 1987.4 nm (where only the fundamental is on-resonance and $\Delta m' = 2.24$). As in Fig. 3, there are local maxima in η when either the fundamental or the SH are resonant with the microdisk cavity. SH conversion is maximized at 1987.4 nm since the value of $\Delta m'$ is close to 2, but conversion at this wavelength is only one or two orders of magnitude larger than other peaks. In contrast, the global maximum in conversion efficiency when the resonances overlap (Fig. 3) can be four or more orders of magnitude larger than other peaks.

By increasing the microdisk radius to 2.643 μm, doubly resonant SHG can be achieved at a pumping wavelength of 2186.9 nm with $\Delta m = -2$ (Fig. 5). At this wavelength, η = 0.29%. The difference in maximum η between this case and the R = 2.609 μm case is due to different values of K_+ and K_- (see Table 1 in Appendix B). Other peaks in SH conversion are produced at wavelengths where only the fundamental or only the SH wave is on-resonance. For instance, a local maximum occurs at λ_f = 2016.7 nm where the fundamental is on-resonance (m_f = 13) while the SH is not. At this pumping wavelength, $\Delta m' = 1.61$ and $\eta = 6.5 \times 10^{-4}\%$.

Figure 6 shows details of the SH conversion spectra for these three microdisk sizes in two different pumping-wavelength ranges. Figure 6a plots conversion efficiency near a pump wavelength of 2000 nm where $\Delta m' \approx 2$. For the R = 2.609 μm disk, the fundamental and SH resonances are aligned and very large SH conversion is achieved (η = 1.2%). For the other disk sizes, the fundamental (m_f = 13) and SH (m_{SH} = 28) resonances become misaligned, resulting in decreased SH conversion. Figure 6b plots the conversion near 2190 nm pumping wavelength where $\Delta m' \approx -2$. Overlapping fundamental and SH resonances are obtained with the R = 2.643 μm disk, resulting in high SH conversion (η = 0.29%).

#149422 - $15.00 USD Received 20 Jun 2011; revised 25 Jul 2011; accepted 25 Jul 2011; published 15 Aug 2011

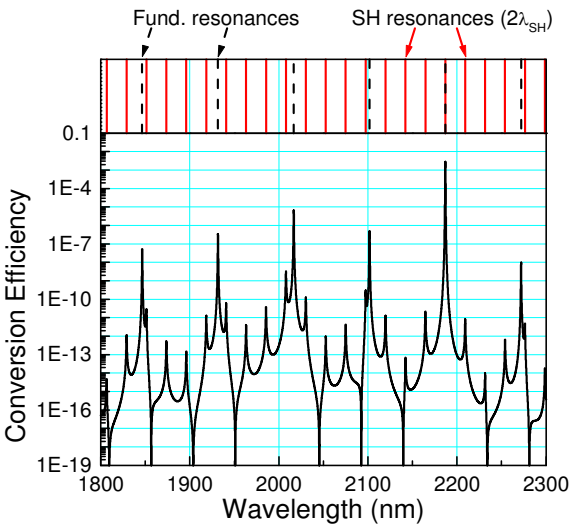

Fig. 5. SH conversion efficiency for various pumping wavelengths in a GaAs microdisk (R = 2.643 μm, h = 161nm). Doubly resonant SHG is achieved at $\lambda_f = 2\lambda_{SH}$ = 2186.9 nm where m_f = 11, m_{SH} = 20, Δm = –2; and SH conversion is maximized with η = 0.29% (P_f^{in} = 1 mW). The top inset shows locations of the fundamental and SH ($2\lambda_{SH}$) cavity resonances.

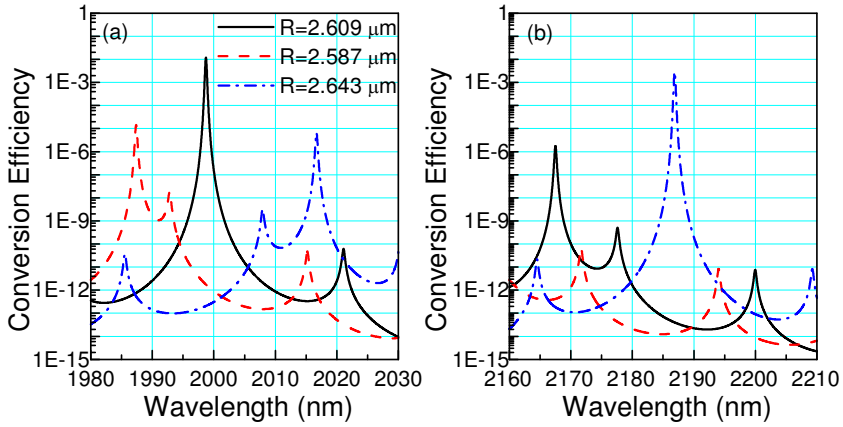

Fig. 6. Detailed pump-wavelength dependence of SH conversion efficiency for three different GaAs microdisk sizes (h = 161nm). (a) Double resonance satisfying Δm = 2 is achieved at $\lambda_f = 2\lambda_{SH}$ = 1998.7 nm in the 2.609-μm-radius disk, and (b) double resonance satisfying Δm = –2 is achieved at $\lambda_f = 2\lambda_{SH}$ = 2186.9 nm in the 2.643-μm-radius disk.

Maximum SHG is obtained when the fundamental and SH resonances overlap and have azimuthal numbers that satisfy $\Delta m = m_{SH} - 2m_f = \pm 2$. As the disk radius, thickness or temperature is changed, the resonances no longer coincide and $\Delta m' \neq \pm 2$, which reduces SHG. Figure 7 illustrates the effect of radius and temperature tuning on SH conversion. The reference microdisk has 161-nm thickness and R_0 = 2.609 μm, and supports doubly resonant SHG at $\lambda_f = 2\lambda_{SH}$ = 1998.7 nm (m_f = 13, m_{SH} = 28). By changing the radius of the microdisk by 5 nm, the fundamental and SH resonances become detuned by $|\lambda_f - 2\lambda_{SH}|$ = 1.3 nm (several times the 0.4 nm linewidth of these $Q_f = Q_{SH}$ = 5000 resonances), and the maximum SH conversion efficiency drops from 1.2% to 2.8×10^{-2}% (see Fig. 7a). Temperature can be used for fine tuning, as shown in Fig. 7b. Maximum conversion is obtained at T = 30 °C while at T = 10 °C or 50 °C, the fundamental and SH resonances are detuned by $|\lambda_f - 2\lambda_{SH}|$ = 0.5 nm, resulting in a sevenfold decrease in peak SH conversion. The curves become noticeably

#149422 - $15.00 USD Received 20 Jun 2011; revised 25 Jul 2011; accepted 25 Jul 2011; published 15 Aug 2011

asymmetric as the fundamental and SH resonances only partially overlap. Varying the geometry or temperature also changes the strength of the interaction through K_+ and K_-, but the SH conversion is more strongly affected by the detuning of the resonances (for this example, changing the microdisk radius by 5 nm changes the magnitudes of K_+ and K_- by only 0.2%).

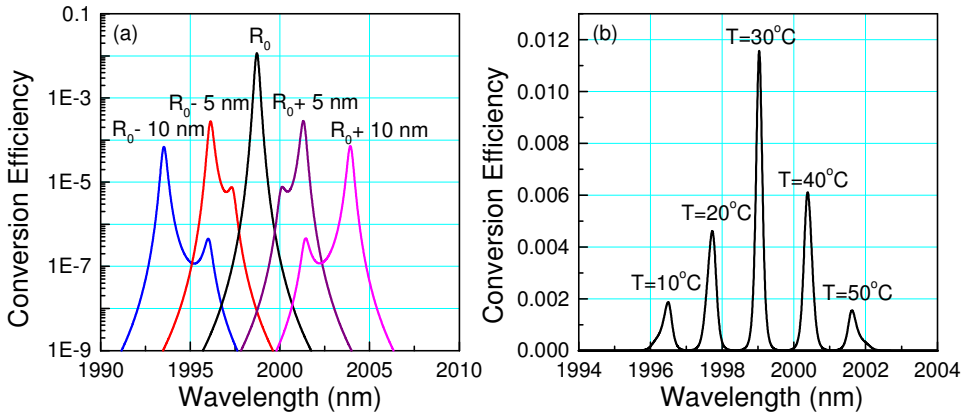

Fig. 7. (a) Varying disk radius around R_0 = 2.609 μm for fixed disk thickness of 161 nm. When the radius is changed by ± 5 nm, the resonances become detuned by $|\lambda_f - 2\lambda_{SH}|$ = 1.3 nm (linewidths of passive cavity resonances are 0.4 nm), which results in a 41-fold reduction in maximum conversion efficiency. (b) Temperature tuning in a R_0 = 2.609 μm, h = 161 nm GaAs microdisk. At T = 10 °C and 50 °C, fundamental and SH resonances are separated by $|\lambda_f - 2\lambda_{SH}|$ = 0.5 nm and the peak conversion efficiency is seven times smaller than the peak at T = 30 °C.

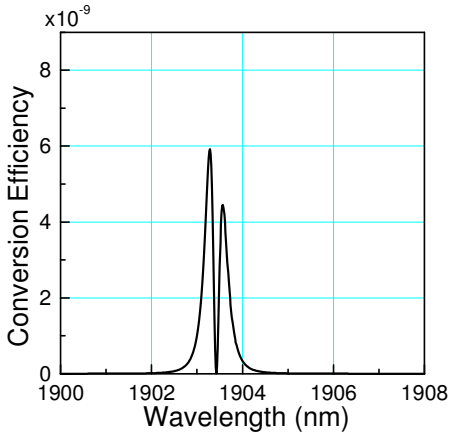

Fig. 8. Overlapping fundamental and SH resonances ($\lambda_f = 2\lambda_{SH}$) occur in a 2.587-μm-radius, 161-nm-thick GaAs microdisk, but Δm = 4 (m_f = 14, m_{SH} = 32), which results in a suppression of SHG due to perfectly destructive $\bar{4}$-QPM.

It is possible for the fundamental and SH resonances of a microdisk to be aligned but Δm is not equal to ±2 but another integer instead. This situation occurs in a 2.587-μm radius, 161-nm-thick GaAs microdisk at a pumping wavelength of 1903.4 nm, shown in Fig. 4 with a detailed plot in Fig. 8. SHG is suppressed when Δm = 0, ±1, ±3, etc. due to perfectly destructive $\bar{4}$-quasi-phasematching. The width of the dip is comparable to the linewidths of the passive cavity resonances (discussed in Section 4). This feature is interesting from an experimental standpoint. It is difficult to measure directly the m values of the resonances, but the presence of the dip clearly indicates that $\Delta m \neq \pm 2$. Since the dip arises from perfectly

#149422 - $15.00 USD Received 20 Jun 2011; revised 25 Jul 2011; accepted 25 Jul 2011; published 15 Aug 2011

balanced destructive interference of the SH wave, the observed sharpness and depth of the dip can be a measure of the quality of the microdisk (its circularity, uniformity and loss).

4. Discussion

Three effects enhance $\chi^{(2)}$ conversion in a GaAs microdisk — resonance enhancement at the fundamental wave, resonance enhancement at the second-harmonic wave, and $\bar{4}$-quasi-phasematching. SHG is significantly enhanced when all three resonance conditions are satisfied. In the examples discussed in Section 3, up to 1.2% conversion efficiency can be obtained using 1 mW of external fundamental power. Resonantly enhanced SHG in a microdisk is far more efficient than single-pass SHG in a GaAs crystal of comparable size. Confocally focused SHG in a GaAs sample of length $2\pi R = 16\,\mu\text{m}$ only produces $\eta \approx 10^{-6}\%$ with 1mW of incident power. As a side note, Section 3 discusses mixing of lowest-order radial modes, which produces larger η than mixing a fundamental with one radial antinode and a SH with two [11] due to better radial-mode overlap.

It is possible to observe SHG in a GaAs microdisk even if the resonance conditions are not all satisfied. Comparing Eqs. (10), (14), and (15), we see the spectrum of the SHG output has three factors

$$P_{SH}^{out} = |C_{1,SH}|^2 \propto \left|B_{2,f}(\phi_f)\right|^4 \times \left|\tilde{K}\right|^2 \times \left|B_{2,SH,passive}(\phi_{SH})\right|^2 . \tag{20}$$

The first factor is the square of the circulating fundamental spectrum, and the last factor is the circulating SH spectrum of the passive cavity. The middle factor in Eq. (20) is the contribution from the nonlinear mixing, whose spectral dependence is described by Eq. (4). The bandwidth of $|\tilde{K}|^2$ is broad because it is determined by one roundtrip of nonlinear mixing (essentially, $|\tilde{K}|^2 \propto \text{sinc}^2(\Delta k \ell / 2)$ where Δk is the wavevector mismatch and ℓ the length of one cavity roundtrip). The relative spectral overlap between the three factors in Eq. (20) determine the total SH conversion. Since P_{SH}^{out} varies as the square of the circulating fundamental power and linearly with the SH power, resonance enhancement at λ_f has a bigger effect than resonance enhancement at λ_{SH}.

There is a strong analogy between $\bar{4}$-QPM in a microdisk and Fresnel phasematching in a plate [6,7]. The output SH intensity in Fresnel phasematching is proportion to [6,7]

$$I_{SH}^{out} \propto \left[\frac{\sin(\Delta kL/2)}{\Delta kL/2}\right]^2 \left[\frac{\sin(N\varepsilon/2)}{\sin(\varepsilon/2)}\right]^2 , \tag{21}$$

where L is the distance between zigzag bounces, N is the total number of bounces and ε is the phase error accumulated per zigzag path. The first factor in Eq. (21) represents the gain factor while the second factor represents the resonance condition [6]. For small ε, the second factor can be written as [7]

$$\left[\frac{\sin(N\varepsilon/2)}{\sin(\varepsilon/2)}\right]^2 = N^2 \,\text{sinc}^2(N\varepsilon/2). \tag{22}$$

This factor is analogous to the passive-cavity-spectra factors in Eq. (20); more bounces in the plate (i. e., larger N) lead to more SHG while narrowing the generated spectrum in the same way that higher Q_f and Q_{SH} lead to more roundtrips in the cavity, higher circulating powers and narrower spectra. In both Fresnel phasematching and $\bar{4}$-QPM in a microdisk, the gain factors (represented by the first factor in Eq. (21) and the second factor in Eq. (20)) are multiplied by the cavity-resonance factors, much in the same way that a Fabry-Perot cavity resonance interacts with a gain medium [6].

A big difference between Fresnel phasematching and $\bar{4}$-QPM in a microdisk is the presence of the resonant cavity for the latter. Firstly, the microdisk cavity allows for a much

#149422 - $15.00 USD Received 20 Jun 2011; revised 25 Jul 2011; accepted 25 Jul 2011; published 15 Aug 2011

more compact device compared to a Fresnel-phasematched device. Secondly, the cavity enforces high periodicity for long, total path-length. Variations in plate thickness (from roughness or wedge) can lead to large phase error, ε. If the phase error is too large, then the useful net path-length (that is, useful N) is reduced. Large phase errors also reduce the wavelength-acceptance bandwidth.

The high periodicity of the effective domain inversions provided by the microdisk cavity makes microcavity structures attractive for efficient $\overline{4}$-QPM conversion. Curved waveguide structures have also been proposed for $\overline{4}$-QPM [12]. These structures are challenging to fabricate since the length of each domain inversion can vary due to fabrication errors. The domain-length errors are similar to phase errors in Fresnel phasematching; both types of errors will reduce the net conversion efficiency and reduce the wavelength-acceptance bandwidth.

Equations (14) and (15) describe very well $\overline{4}$-quasi-phasematched SHG in a microdisk for cases where either the fundamental or SH wave is not resonant with the cavity. We can also give an intuitive description for this process. If light is not resonant with a cavity, then there is destructive interference between the incident and circulating waves, which results in suppression of light circulating inside the cavity. However, due to finite quality factors, the amount of light inside the cavity is non-zero even if the wave is off-resonance. If the fundamental wave is resonant with the cavity, then the circulating intensity inside the cavity at λ_f will be high. This light can initiate second-harmonic generation at the entrance of the cavity. The second-harmonic will increase due to $\overline{4}$-QPM as it propagates around the cavity and if the SH is resonant with the cavity, then the SH light from previous round trips will add constructively to subsequent round trips. However, if the SH light is not resonant with the cavity, then some amount of SH is coupled out, and the remaining SH inside the cavity interferes destructively with light from previous round trips. In essence, when the SH wave is off-resonance with the cavity, there is negligible λ_{SH} light at the entrance of the cavity, and the net amount of SH generated is essentially the amount produced on one round trip times the out-coupling coefficient. Having the fundamental wave resonant with the cavity will significantly increase SHG since the driving fields will be large (due to resonance enhancement). Conversely, if the fundamental is not resonant with the cavity, but $\lambda_f/2$ matches a cavity resonance, then there will still be an enhancement of SHG in the cavity. Since Q_f is finite, there will be some small amount of fundamental light in the cavity and this light can initiate SHG. The generated second-harmonic light is resonant with the cavity and will experience build-up as SH light from subsequent round-trips add constructively.

Equation (2) implies that a perfectly circular cavity has only two components that can contribute to quasi-phasematching: $\Delta m = \pm 2$. It would be interesting to explore square [11] or deformed cavities [21,22] that would provide resonance enhancement of the circulating waves and allow higher-order QPM. The deformed cavities would have interesting applications with free-space couplers because of their directional output.

When $\Delta m = 0, \pm 1, \pm 3$, etc. in a circular cavity, SHG is suppressed due to perfectly destructive $\overline{4}$-QPM (Fig. 8). In this process, each round trip in the cavity produces no net SH, similar to the way there is no net SH is produced after exactly two coherence lengths in a non-phasematched crystal. This suppression is analogous to operating a nonlinear crystal at $\eta \propto \text{sinc}^2(\Delta kL/2) = 0$, which occurs when $\Delta kL/2 = \pm \pi, \pm 2\pi$, etc. We can derive an expression for the width of the destructive $\overline{4}$-QPM dip when the fundamental and SH resonances overlap ($\lambda_f = 2\lambda_{SH}$) and $\Delta m = 0, \pm 1, \pm 3$, etc. In the vicinity of the dip, $|\tilde{K}|^2 \propto (\lambda - \lambda_0)^2$ since the sinc^2 function varies quadratically near its zeros. The circulating power spectrum of the fundamental and SH resonances (Eq. (10)) can be approximated by Lorentzian lineshapes with FWHM widths w_f and w_{SH}, respectively (in wavelength units). If $w_f = 2w_{SH}$ (same total quality factors for both waves), then the width of the destructive $\overline{4}$-QPM dip is $0.31w_f$. The sharpness of a measured, destructive $\overline{4}$-QPM dip where $\Delta m \neq \pm 2$ can be used to characterize the circularity and ideality of a microdisk.

#149422 - $15.00 USD Received 20 Jun 2011; revised 25 Jul 2011; accepted 25 Jul 2011; published 15 Aug 2011

5. Conclusions

We have presented a theory of $\bar{4}$-quasi-phasematched second-harmonic generation in a GaAs microdisk that describes both on- and off-resonance conversion. For doubly resonant mixing of lowest-order vertical and radial modes satisfying $m_f = 13$, $m_{SH} = 28$ and $\Delta m = 2$ in a 2.609-μm-radius, 161-nm-thick microdisk, the theory predicts 1.2% conversion efficiency with 1 mW of $\lambda_f = 1998.7$ nm external fundamental light (assuming critical coupling and $Q_f = Q_{SH} = 5000$). Our theory also describes SHG when the fundamental and SH resonances no longer overlap ($\lambda_f - 2\lambda_{SH} \neq 0$), and SHG is no longer doubly resonant. When $|\lambda_f - 2\lambda_{SH}| = 1.3$ nm, we expect a maximum conversion efficiency of $\eta = 2.8 \times 10^{-2}$% and when $|\lambda_f - 2\lambda_{SH}| = 5.4$ nm, we expect $\eta = 1.4 \times 10^{-3}$% (for $Q_f = Q_{SH} = 5000$, the linewidths of the passive-cavity resonances are 0.4 nm). We show that the SH conversion spectrum is a product of the circulating-power cavity spectra at the fundamental and SH wavelengths, and the nonlinear gain spectrum, $|\tilde{K}|^2$. In analogy to Fresnel phasematching, narrowing the passive cavity spectra (through higher Q) is associated with longer total interaction length and higher conversion. Higher quality factors also lead to tighter fabrication tolerances for achieving the double-resonance condition ($\lambda_f = 2\lambda_{SH}$). Using a series of lower-quality-factor, waveguide-coupled GaAs microdisks would allow higher nonlinear conversion with broader spectral bandwidth [23]. We also identify the process of perfectly destructive $\bar{4}$-QPM; SHG is suppressed in a circular GaAs microdisk at the wavelengths where $\Delta m' = 0, \pm 1, \pm 3$, etc. In this process, there is destructive interference of the second-harmonic wave, which result in no net SHG per cavity round-trip and a dip in the SH conversion spectrum. This dip can be used to confirm $\Delta m \neq \pm 2$ and to evaluate the circularity and ideality of the microdisk.

Appendix A. Derivation of second-harmonic generation coefficients

In this appendix, we derive the SHG coefficients (K_+ and K_-) used in Section 2. Calculations of the whispering gallery modes and their normalization conditions are reviewed. We describe the power normalization of the fields, where $|A_i(\theta)|^2$ represents the circulating power inside the microdisk. The fields can also be normalized to represent stored energy, which is used in coupled-mode theory [11,24] (Appendix B).

A.1 Stationary eigenmodes

The eigenmodes of a microdisk can be approximated by the analytical expressions presented in Ref [25], which we will summarize here. In a thin microdisk with surface normal $\hat{z}$, the fields naturally decouple into transverse electric (TE, $\{H_z, E_r, E_\theta\}$) and transverse magnetic (TM, $\{E_z, H_r, H_\theta\}$) polarizations. By using Maxwell's equations, the radial and azimuthal components can be derived from the z-components (H_z or E_z)

$$\begin{aligned} &\mathrm{TM} = \{E_z, H_r, H_\theta\} && \mathrm{TE} = \{H_z, E_r, E_\theta\} \\ &H_r = \frac{m}{r\mu_0\omega} E_z && E_r = -\frac{m}{r\varepsilon_0 n^2 \omega} H_z \\ &H_\theta = \frac{1}{i\mu_0\omega}\frac{\partial E_z}{\partial r} && E_\theta = \frac{i}{\varepsilon_0 n^2 \omega}\frac{\partial H_z}{\partial r} \end{aligned} \quad . \tag{23}$$

The field F_z (where $F_z = H_z$ or E_z) is separable and can be written as

$$F_z \exp(i\omega t) = A(\theta)\psi(r)Z(z)\exp[i(\omega t - m\theta)]. \tag{24}$$

Using Eq. (24), Maxwell's wave equation in cylindrical coordinates becomes three differential equations

#149422 - $15.00 USD Received 20 Jun 2011; revised 25 Jul 2011; accepted 25 Jul 2011; published 15 Aug 2011

$$\frac{\partial^2 Z}{\partial z^2} + k_0{}^2(n^2 - \overline{n}^2)Z = 0$$
$$\frac{\partial^2 \psi}{\partial r^2} + \frac{1}{r}\frac{\partial \psi}{\partial r} + k_0{}^2\overline{n}^2\psi = \frac{l^2}{r^2}\psi\,, \tag{25}$$
$$\frac{\partial^2 A}{\partial \theta^2} - 2im\frac{\partial A}{\partial \theta} - m^2 A = -l^2 A$$

where $k_0 = \omega/c$ is the vacuum wavevector and $n = n(\boldsymbol{r})$ is the refractive index. If we take the slowly varying envelope approximation (SVEA) so that $\partial^2 A/\partial\theta^2 = \partial A/\partial\theta = 0$, then the last equation implies $l = m$ and $A(\theta)$ is approximately constant.

The vertical dependence, $Z(z)$, can be solved by considering a slab-waveguide model [26], which yields an effective index, $\overline{n}$. The slab can support multiple modes, which are indexed by an integer $q = 1, 2,\ldots$ that counts the number of vertical antinodes. We should therefore write the effective index as $\overline{n}_q$. The functional form of $Z(z)$ involves real functions: exponentials, sines and cosines [26].

The unnormalized radial dependence is approximated by

$$\psi(r) = \begin{cases} J_m(k_0\overline{n}_q r) & r < R \\ J_m(k_0\overline{n}_q R)\exp(-\tilde{\alpha}(r-R)) & r > R \end{cases}, \tag{26}$$

where R is the disk radius, $J_m(k_0\overline{n}_q r)$ is the Bessel function of the first kind and $\tilde{\alpha} = k_0(\overline{n}_q{}^2 - n^2)^{1/2}$ [25]. The decaying exponential for $r>R$ is an approximation for the actual solution, which is the Hankel function of the second kind: $H_m{}^{(2)}(k_0\overline{n}_q r)$ [9]. We match boundary conditions to solve for the resonant wavelength where Eq. (25) is a valid solution. Equation (26) incorporates the first boundary condition that $\psi(r)$ is continuous at $r = R$ (i. e., H_z and E_z are continuous at the disk boundary). The other boundary condition is that the tangential fields are continuous; that is [25]

$$\begin{array}{ll} \text{TM}: H_\theta \text{ is continuous} & \text{TE}: E_\theta \text{ is continuous} \\ \left.\dfrac{\partial E_z}{\partial r}\right|_{r<R} = \left.\dfrac{\partial E_z}{\partial r}\right|_{r>R} & \left.\dfrac{1}{n^2}\dfrac{\partial H_z}{\partial r}\right|_{r<R} = \left.\dfrac{\partial H_z}{\partial r}\right|_{r>R}. \end{array} \tag{27}$$

We assume that $n = 1$ outside the microdisk. These boundary conditions allow us to find the resonant wavelengths by solving the following transcendental equations

$$\begin{aligned} &\text{TM:}\quad J_m(k_0\overline{n}_q R)\left[\frac{m}{R} + \tilde{\alpha}\right] = k_0\overline{n}_q J_{m+1}(k_0\overline{n}_q R) \\ &\text{TE:}\quad J_m(k_0\overline{n}_q R)\left[\frac{m}{R} + \tilde{\alpha}\left(\frac{\overline{n}}{n}\right)^2\right] = k_0\overline{n}_q J_{m+1}(k_0\overline{n}_q R)\,. \end{aligned} \tag{28}$$

There are multiple solutions to Eq. (28) indexed by the number of radial antinodes, p, in $\psi(r)$.

Solving Eq. (28) gives us the wavelengths of the resonant modes, λ_{mpq}. Both $Z_q(z)$ and $\psi_p(r)$ are not normalized. They can be inserted into expressions for H_z and E_z (Eq. (24)), which can then be normalized to determine the constant $A(\theta)$.

A.2 Normalization of eigenmodes

The eigenmodes may be normalized such that $|A(\theta)|^2$ represents the circulating power inside the microdisk. The generalized waveguide-microresonator theory in Section 2 uses this normalization. For clarity, let $\tilde{Z}_q(z)$ and $\tilde{\psi}_p(r)$ represent normalized functions, which are related to the unnormalized functions $Z_q(z)$ and $\psi_p(r)$ by

#149422 - $15.00 USD Received 20 Jun 2011; revised 25 Jul 2011; accepted 25 Jul 2011; published 15 Aug 2011

$$\begin{matrix}\tilde{\psi}_p(r)=c_p\psi_p(r)\\ \tilde{Z}_q(z)=d_qZ_q(z)\end{matrix}. \tag{29}$$

The circulating power, P_{circ}, of the microdisk is

$$P_{circ}=\mathbf{P}\cdot\hat{\theta}=\frac{1}{2}\int(\mathbf{E}\times\mathbf{H}^*)\cdot\hat{\theta}\,drdz. \tag{30}$$

The integration is performed over the cross-sectional area of the microdisk and includes the evanescent field extending slightly outside the disk. For the power normalization, $P_{circ} = |A(\theta)|^2$, which implies

$$\begin{aligned}\text{TM: }\ & P_{circ}=\frac{1}{2}\iint E_zH_r^*drdz=\left|A(\theta)\right|^2\\ & \frac{m}{2\mu_0\omega}\iint\frac{1}{r}\left|\tilde{\psi}_p(r)\tilde{Z}_q(z)\right|^2drdz=1\\ \text{TE: }\ & P_{circ}=-\frac{1}{2}\iint H_z^*E_rdrdz=\left|A(\theta)\right|^2\\ & \frac{m}{2\varepsilon_0n^2\omega}\iint\frac{1}{r}\left|\tilde{\psi}_p(r)\tilde{Z}_q(z)\right|^2drdz=1.\end{aligned} \tag{31}$$

The double integral over r and z separates into two normalization equations. We can set the integral over z to unity and obtain the following conditions

$$\begin{aligned}&\int_{-\infty}^{\infty}\left|\tilde{Z}_q(z)\right|^2dz=1\\ &\text{TM: }\ \frac{m}{2\mu_0\omega}\int_0^{\infty}\frac{1}{r}\left|\tilde{\psi}_p(r)\right|^2dr=1\\ &\text{TE: }\ \frac{m}{2\varepsilon_0n^2\omega}\int_0^{\infty}\frac{1}{r}\left|\tilde{\psi}_p(r)\right|^2dr=1.\end{aligned} \tag{32}$$

We note that $Z_q(z)$ and $\psi_p(r)$ constructed in section A.1 are real, so the absolute value in Eq. (32) is not needed.

A.3 Nonlinear optical coupling

Nonlinear interactions between the modes of the microdisk can be described using a perturbative approach [27]. The eigenmodes, as described in Section A.1, obey the unperturbed wave equation

$$\nabla^2\mathbf{E}-\mu\varepsilon\frac{\partial^2\mathbf{E}}{\partial t^2}=0, \tag{33}$$

where $\mu = \mu_0$ (for a non-magnetic material), $\varepsilon = \varepsilon_0 n^2$ inside the microdisk, and $\varepsilon = \varepsilon_0$ outside the disk. We can introduce a perturbing polarization source arising from the nonlinear interaction, $\mathbf{P}^{NL}$, which produces a perturbed wave equation

$$\nabla^2\mathbf{E}-\mu\varepsilon\frac{\partial^2\mathbf{E}}{\partial t^2}=\mu_0\frac{\partial^2\mathbf{P}^{NL}}{\partial t^2}. \tag{34}$$

The eigenmodes that solve the unperturbed wave equation (Eq. (33)) form a complete, mutually orthogonal set, and therefore the solution to Eq. (34) can be written as a linear combination of these eigenmodes.

Let us consider SHG with a TE-polarized fundamental and a TM-polarized second harmonic. The SH field that satisfies Eq. (34), E_z, can be written as a sum over the TM-polarized SH eigenmodes that solved the unperturbed equation:

#149422 - $15.00 USD Received 20 Jun 2011; revised 25 Jul 2011; accepted 25 Jul 2011; published 15 Aug 2011

$$E_z = \sum_{m'_{SH},p'_{SH},q'_{SH}} A_{m'_{SH}\ p'_{SH}\ q'_{SH}}(\theta)\tilde{\psi}_{m'_{SH}\ p'_{SH}\ q'_{SH}}(r)\tilde{Z}_{q'_{SH}}(z)e^{i(\omega_{SH}t-m'_{SH}\theta)} + \text{radiation modes} \quad (35)$$

The terms $A_{m'_{SH}\ p'_{SH}\ q'_{SH}}(\theta)$ are slowly-varying envelope functions and act like the weighting factors. We have explicitly written out the indices associated with the constituent functions. For this analysis, we neglect the effect of the radiation modes since we are more interested in the guided modes of the microdisk.

Equation (35) can be substituted into Eq. (34), and many of the terms will sum to zero because the constituent functions are all solutions to the homogeneous equation, Eq. (33). The only remaining terms are those that involve the derivatives of $A_{m'_{SH}\ p'_{SH}\ q'_{SH}}(\theta)$ and the z-component of the nonlinear polarization:

$$\sum_{m'_{SH},p'_{SH},q'_{SH}} \frac{1}{r^2}\left(\frac{\partial^2 A_{m'_{SH}\ p'_{SH}\ q'_{SH}}}{\partial\theta^2} - 2im'_{SH}\frac{\partial A_{m'_{SH}\ p'_{SH}\ q'_{SH}}}{\partial\theta}\right)\times \tilde{\psi}_{m'_{SH}\ p'_{SH}\ q'_{SH}}(r)\tilde{Z}_{q'_{SH}}(z)e^{i(\omega_{SH}t-m'_{SH}\theta)} = -\mu_0\omega_{SH}{}^2 P_z^{NL}. \quad (36)$$

Since $\left|\partial^2 A_{m'_{SH}}/\partial\theta^2\right| \ll \left|2m'_{SH}\partial A_{m'_{SH}}/\partial\theta\right|$ (SVEA), the first term in the parentheses can be neglected. We also assumed the nonlinear polarization oscillates at frequency ω_{SH} so that $\partial^2 P_z^{NL}/\partial t^2 \approx -\omega_{SH}{}^2 P_z^{NL}$. We can now utilize the orthogonality of the eigenmodes [28]

$$\int_{-\infty}^{\infty}\int_0^{2\pi}\int_0^{\infty} F_{z,mpq}\frac{F_{z,m'p'q'}}{r}drd\theta dz \propto \delta_{mm'}\delta_{pp'}\delta_{qq'}, \quad (37)$$

where $F_z = H_z$ or E_z, and "project out" the coefficients associated with (m_{SH}, p_{SH}, q_{SH}) by multiplying both sides of Eq. (36) by $r\tilde{\psi}_{m_{SH}\ p_{SH}\ q_{SH}}(r)\tilde{Z}_{q_{SH}}(z)e^{im_{SH}\theta}$ and integrating over all θ, r and z:

$$\int_{-\infty}^{\infty}\int_0^{2\pi}\int_0^{\infty}\sum_{m'_{SH},p'_{SH},q'_{SH}}\left(-2im'_{SH}\frac{\partial A_{m'_{SH}}}{\partial\theta}\right)\left(\tilde{\psi}_{m'_{SH}\ p'_{SH}\ q'_{SH}}(r)\frac{\tilde{\psi}_{m_{SH}\ p_{SH}\ q_{SH}}(r)}{r}\right)\times \tilde{Z}_{q'_{SH}}(z)\tilde{Z}_{q_{SH}}(z)e^{i(m_{SH}-m'_{SH})\theta}drd\theta dze^{i\omega_{SH}t} = -\mu_0\omega_{SH}{}^2\int_{-\infty}^{\infty}\int_0^{2\pi}\int_0^{\infty} P_z^{NL}r\tilde{\psi}_{m_{SH}\ p_{SH}\ q_{SH}}(r)\tilde{Z}_{q_{SH}}(z)e^{im_{SH}\theta}drd\theta dz. \quad (38)$$

Since $A_{m'_{SH}\ p'_{SH}\ q'_{SH}}$ is the slowly varying envelope, its derivative $\partial A_{m'_{SH}\ p'_{SH}\ q'_{SH}}/\partial\theta$ is essentially a constant with respect to θ, so the $\int_0^{2\pi} e^{i(m_{SH}-m'_{SH})\theta}d\theta$ integral acts like the Kronecker delta function, $\delta_{m'_{SH}m_{SH}}$. The integral over θ on the left-hand side of Eq. (38) is

$$\sum_{m'_{SH}}\int_0^{2\pi}\frac{\partial A_{m'_{SH}\ p'_{SH}\ q'_{SH}}}{\partial\theta}e^{i(m_{SH}-m'_{SH})\theta}d\theta \approx 2\pi\frac{\partial A_{m_{SH}\ p'_{SH}\ q'_{SH}}}{\partial\theta}. \quad (39)$$

The r and z integrals on the left-hand side of Eq. (38) select out the terms $p'_{SH} = p_{SH}$ and $q'_{SH} = q_{SH}$. The integral can be simplified using the normalization expressions. Using Eq. (32) so that $\left|A_{m_{SH}\ p_{SH}\ q_{SH}}\right|^2$ represent power, Eq. (38) becomes

#149422 - $15.00 USD Received 20 Jun 2011; revised 25 Jul 2011; accepted 25 Jul 2011; published 15 Aug 2011

$$-4\pi i m_{SH}\frac{\partial A_{m_{SH}\,p_{SH}\,q_{SH}}}{\partial\theta}\left(\frac{2\mu_0\omega_{SH}}{m_{SH}}\right)e^{i\omega_{SH}t}= -\mu_0\omega_{SH}{}^2\int_{-\infty}^{\infty}\int_0^{2\pi}\int_0^{\infty}P_z^{NL}r\tilde{\psi}_{m_{SH}\,p_{SH}\,q_{SH}}(r)\tilde{Z}_{q_{SH}}(z)e^{im_{SH}\theta}drd\theta dz\,. \tag{40}$$

In GaAs and other crystals with $\bar{4}3m$ point-group symmetry, the only non-zero nonlinear-susceptibility-tensor elements are $d_{14} = d_{25} = d_{36} = d_{zxy}$ so the z-component of $\mathbf{P}^{NL}$ is

$$P_z^{NL} = 2\varepsilon_0 d_{14}E_x^f E_y^f\,. \tag{41}$$

In terms of E_r and E_θ,

$$\begin{aligned}E_x &= E_r\cos\theta - E_\theta\sin\theta\\ E_y &= E_r\sin\theta + E_\theta\cos\theta\,,\end{aligned} \tag{42}$$

so that

$$P_z^{NL} = 2\varepsilon_0 d_{14}\left[\cos 2\theta\,E_r^f E_\theta^f + \frac{1}{2}\sin 2\theta(E_r^{f\,2} - E_\theta^{f\,2})\right]. \tag{43}$$

From Eq. (23), E_r^f and E_θ^f are proportional to H_z^f and $\partial H_z^f/\partial r$, respectively, which are both proportional to $e^{-im_f\theta}$. The sine and cosine terms in Eq. (43) produce factors of $e^{i2\theta}$ and $e^{-i2\theta}$, so P_z^{NL} is proportional to $e^{i(-2m_f+2)\theta}$ and $e^{i(-2m_f-2)\theta}$.

If we let $\tilde{\psi}_{SH} = \tilde{\psi}_{m_{SH}\,p_{SH}\,q_{SH}}(r)$, then combining and rearranging Eqs. (23), (24), (40) and (43), we see that

$$\begin{aligned}&2\pi\frac{\partial A_{m_{SH}\,p_{SH}\,q_{SH}}}{\partial\theta} =\\ &\quad\frac{-d_{14}}{2\varepsilon_0\omega_{SH}}\left(\frac{A_{m_f p_f q_f}}{n_f{}^2}\right)^2\int_{-h/2}^{h/2}\tilde{Z}_{q_{SH}}(z)\tilde{Z}_{q_f}^2(z)dz\times\\ &\qquad\int_0^{2\pi}\left[\begin{array}{l}\displaystyle\int_0^R e^{i(\Delta m+2)\theta}r\tilde{\psi}_{SH}\left(\frac{m_f}{r}\tilde{\psi}_f+\frac{\partial\tilde{\psi}_f}{\partial r}\right)^2 dr\\ \displaystyle\quad-\int_0^R e^{i(\Delta m-2)\theta}r\tilde{\psi}_{SH}\left(\frac{m_f}{r}\tilde{\psi}_f-\frac{\partial\tilde{\psi}_f}{\partial r}\right)^2 dr\end{array}\right]d\theta\end{aligned} \tag{44}$$

where $\Delta m = m_{SH} - 2m_f$. Note that the limits of integration are [0,R] for r and [-h/2, h/2] for z (where R and h are the radius and height of the microdisk) since the nonlinearity, d_{14}, is only non-zero inside the disk. For good vertical mode overlap, $\tilde{Z}_{q_f}^2(z)\propto\tilde{Z}_{q_{SH}}(z)$ (i.e., the shape of $\tilde{Z}_{q_f}^2(z)$ should match that of $\tilde{Z}_{q_{SH}}(z)$).

We had approximated that $\partial A_{m_{SH}\,p_{SH}\,q_{SH}}/\partial\theta$ is a constant with respect to θ, so the left-hand side is actually $\int_0^{2\pi}\left(\partial A_{m_{SH}\,p_{SH}\,q_{SH}}/\partial\theta\right)d\theta$. Terms on the right-hand side of Eq. (44) can be collected and we identify

$$\frac{\partial A_{m_{SH}\,p_{SH}\,q_{SH}}}{\partial\theta} = A_{m_f p_f q_f}^2\left(K_+e^{i(\Delta m+2)\theta}+K_-e^{i(\Delta m-2)\theta}\right), \tag{45}$$

#149422 - $15.00 USD Received 20 Jun 2011; revised 25 Jul 2011; accepted 25 Jul 2011; published 15 Aug 2011

where

$$K_{+}^{pow} = -\frac{d_{14}}{2\varepsilon_0 \omega_{SH} n_f^4} \int_{-h/2}^{h/2} \tilde{Z}_{q_{SH}}(z) \tilde{Z}_{q_f}^2(z) dz \int_0^R r \tilde{\psi}_{SH} \left(\frac{m_f}{r} \tilde{\psi}_f + \frac{\partial \tilde{\psi}_f}{\partial r} \right)^2 dr$$
$$K_{-}^{pow} = \frac{d_{14}}{2\varepsilon_0 \omega_{SH} n_f^4} \int_{-h/2}^{h/2} \tilde{Z}_{q_{SH}}(z) \tilde{Z}_{q_f}^2(z) dz \int_0^R r \tilde{\psi}_{SH} \left(\frac{m_f}{r} \tilde{\psi}_f - \frac{\partial \tilde{\psi}_f}{\partial r} \right)^2 dr . \quad (46)$$

$K_{\pm}^{pow}$ in Eq. (46) are labeled by the *pow* superscript to indicate that they are calculated using the power normalization of the fields.

The quasi-phasematching condition can be seen in Eq. (45): the sinusoidally varying portion of $\partial A_{m_{SH}\, p_{SH}\, q_{SH}} / \partial \theta$ vanishes if $\Delta m = m_{SH} - 2m_f = \pm 2$. Equation (45) differs from Eq. (2) in Ref [11]. by a factor *i* since here, P_z^{NL} is shown to be imaginary.

We note that the integral over the vertically varying wavefunctions can be approximated by a simple expression if the unnormalized functions are related by $Z_{q_{SH}}(z) = Z_{q_f}^2(z)$:

$$\int_{-h/2}^{h/2} \tilde{Z}_{q_{SH}}(z) \tilde{Z}_{q_f}^2(z) dz \approx \frac{d_{q_f}^2}{d_{q_{SH}}}, \quad (47)$$

where the constants d_{q_i} are defined in Eq. (29). We found that Eq. (47) is a good approximation when $\tilde{Z}_{q_f}(z)$ and $\tilde{Z}_{q_{SH}}(z)$ are the lowest-order vertical modes.

Appendix B. Conversion efficiency and coupled-mode theory

In this appendix, we derive the conversion efficiency for SHG in microdisks based on coupled-mode theory (CMT) [29]. In CMT, $|A(\theta)|^2$ represents the stored energy inside the resonator rather than the circulating power. We describe energy normalization of the fields and its effect on the SHG coefficients (K_+ and K_-). We calculate the conversion efficiency using CMT and show it agrees with results from Section 2 that were based on the generalized waveguide-microresonator theory (GWMT).

B.1 Energy normalization and SHG coefficients

To have $|A(\theta)|^2$ represent the stored energy, *W*, we can relate P_{circ} to *W* by [29]

$$P_{circ} = \frac{W}{\ell} v_g = \frac{|A|^2}{\ell} v_g . \quad (48)$$

ℓ is the length of the resonator and v_g is the group velocity. The group velocity of waves in a microdisk is [30]

$$v_g = r \delta \omega_{FSR} , \quad (49)$$

where *r* is the radial coordinate inside the microdisk, and $\delta\omega_{FSR}$ is the angular-frequency separation between adjacent modes or the free-spectral range (FSR). Equation (49) implies that the group velocity of the wave depends on its radial location in the disk. However, ℓ also depends on *r* through $\ell = 2\pi r$. Thus the ratio v_g/ℓ is independent of *r* and

$$P_{circ} = |A|^2 \delta f_{FSR} , \quad (50)$$

#149422 - $15.00 USD Received 20 Jun 2011; revised 25 Jul 2011; accepted 25 Jul 2011; published 15 Aug 2011

where $\delta f_{FSR} = \delta\omega_{FSR}/2\pi$ is the FSR in frequency units. Combining Eqs. (30) and (50), we obtain the energy normalization:

$$\begin{aligned}
&\int_{-\infty}^{\infty}\left|\tilde{Z}_q(z)\right|^2 dz = 1 \\
&\text{TM: } \frac{m}{2\mu_0\omega}\int_0^{\infty}\frac{1}{r}\left|\tilde{\psi}_p^{en}(r)\right|^2 dr = \delta f_{FSR} \quad . \\
&\text{TE: } \frac{m}{2\varepsilon_0 n^2\omega}\int_0^{\infty}\frac{1}{r}\left|\tilde{\psi}_p^{en}(r)\right|^2 dr = \delta f_{FSR}
\end{aligned} \tag{51}$$

Here, the normalized radial functions, $\tilde{\psi}_p^{en}(r)$, are given the *en* superscript since they are calculated using the energy normalization of the fields.

Following the procedure outlined in Section A.3 (most notably using Eq. (51) instead of (32) to derive Eq. (40)), the SHG coefficients using the energy normalization are

$$\begin{aligned}
K_+^{en} &= -\frac{d_{14}}{2\varepsilon_0\delta f_{FSR,SH}\omega_{SH}n_f^4}\int_{-h/2}^{h/2}\tilde{Z}_{q_{SH}}(z)\tilde{Z}_{q_f}^2(z)dz\int_0^R r\tilde{\psi}_{SH}^{en}\left(\frac{m_f}{r}\tilde{\psi}_f^{en}+\frac{\partial\tilde{\psi}_f^{en}}{\partial r}\right)^2 dr \\
K_-^{en} &= \frac{d_{14}}{2\varepsilon_0\delta f_{FSR,SH}\omega_{SH}n_f^4}\int_{-h/2}^{h/2}\tilde{Z}_{q_{SH}}(z)\tilde{Z}_{q_f}^2(z)dz\int_0^R r\tilde{\psi}_{SH}^{en}\left(\frac{m_f}{r}\tilde{\psi}_f^{en}-\frac{\partial\tilde{\psi}_f^{en}}{\partial r}\right)^2 dr .
\end{aligned} \tag{52}$$

Numerically, $K_{\pm}^{en}$ can be calculated from $K_{\pm}^{pow}$ (the coefficients calculated using the power normalization, Eq. (46)) using $K_{\pm}^{en} = K_{\pm}^{pow}\delta f_{FSR,f}/\sqrt{\delta f_{FSR,SH}}$.

B.2 Coupled-mode theory

The coupled wave equations describing the fundamental and SH modes in a resonator are [29]

$$\begin{aligned}
\frac{\partial a_f}{\partial t} &= i\omega_f a_f - \left(\frac{1}{\tau_f^0}+\frac{1}{\tau_f^c}\right)a_f + s_f\sqrt{\frac{2}{\tau_f^c}} \\
\frac{\partial a_{SH}}{\partial t} &= i\omega_{SH}a_{SH} - \left(\frac{1}{\tau_{SH}^0}+\frac{1}{\tau_{SH}^c}\right)a_{SH} + s^{NL} .
\end{aligned} \tag{53}$$

a_i is related to A_i (the slowly varying envelope) by

$$a_i = A_i\exp(i\omega_i t) . \tag{54}$$

The fields are normalized so that $|a_i|^2$ and $|A_i|^2$ represent the stored energy. τ_i^0 and τ_i^c are the intrinsic and external coupling photon lifetimes, respectively. The lifetimes are related to the quality factors (Q_i) by $Q_i = \omega_i\tau_i/2$. The total quality factor at wave *i* is given by $1/Q_i = 1/Q_i^0 + 1/Q_i^c$. We assume that the fundamental mode is undepleted and is coupled to an external pump given by $\left|s_f\right|^2 = P_f^{in}$.

Ref [29]. presents the nonlinear source term, s^{NL}, as an overlap integral between the interacting waves and the nonlinear tensor. A more intuitive picture is to cast the nonlinear source in terms of an effective gain time, τ_g, defined by

$$s^{NL} = \frac{a_{SH}}{\tau_g} . \tag{55}$$

#149422 - $15.00 USD Received 20 Jun 2011; revised 25 Jul 2011; accepted 25 Jul 2011; published 15 Aug 2011

In analogy to the usual expression for photon lifetime [29], the gain time is related to the power gained by the resonator according to

$$\frac{2}{\omega_i \tau_g} = \frac{P_{gain}}{\omega_i W_i}, \tag{56}$$

where $W_i = |A_i|^2$ is the stored energy in the resonator at frequency ω_i. By introducing the power-gain coefficient $2\alpha_g$, the power increase through one pass around the resonator (of length ℓ) is

$$P_{gain} = 2\alpha_g \ell P_{circ}. \tag{57}$$

Combining Eqs. (48), (56) and (57), we obtain

$$\tau_g = \frac{1}{\alpha_g v_g}, \tag{58}$$

where v_g is the group velocity in the microdisk (Eq. (49)). In terms of field amplitudes,

$$\alpha_g = \frac{1}{A_{SH}} \frac{dA_{SH}}{r d\theta}, \tag{59}$$

where we abbreviate $A_{SH} = A_{m_{SH}\, p_{SH}\, q_{SH}}$. We can combine Eqs. (45), (49), (54) (55), (58) and (59) to find

$$s^{NL} = a_f^2 \delta\omega_{FSR,SH} K_{\pm}^{en}. \tag{60}$$

$K_{\pm}^{en} = K_{+}^{en}$ if $\Delta m = -2$, and $K_{\pm}^{en} = K_{-}^{en}$ if $\Delta m = +2$ since the dominant contribution to Eq. (45) is from the phasematched component.

The circulating powers and SHG conversion efficiency can be calculated by looking for steady-state solutions to Eq. (53). Utilizing Eq. (50), we find

$$P_f^{circ} = |a_f|^2 \delta f_{FSR,f} = \delta f_{FSR,f} \frac{4Q_f^c}{\omega_f} \frac{1}{(1+Q_f^c/Q_c^0)^2} P_f^{in}. \tag{61}$$

The second-harmonic generated is

$$\begin{aligned} P_{SH}^{out} &= \frac{2}{\tau_{SH}^c} |a_{SH}|^2 \\ &= \frac{4Q_{SH}^c}{\omega_{SH}(1+Q_{SH}^c/Q_{SH}^0)^2} \left(\frac{4Q_f^c}{\omega_f (1+Q_f^c/Q_f^0)^2} P_f^{in} 2\pi\delta f_{FSR,SH} |K_{\pm}^{en}| \right)^2. \end{aligned} \tag{62}$$

Equation (62) can be compared to results of the GWMT discussed in Section 2. If both the fundamental and SH are resonant with the cavity (with $\Delta m = 2$ or -2) and the phase shift from the coupler can be neglected ($\psi_f = \psi_{SH} = 0$), then $\tilde{K}(\varphi_f, \varphi_{SH}) = 2\pi K_{\pm}^{pow}$, and Eq. (15) becomes

$$P_{SH}^{out} = \left(P_f^{in}\right)^2 (1-|t_{SH}|^2) \frac{|2\pi K_{\pm}^{pow}|^2 \alpha_{SH}{}^2}{(1-\alpha_{SH}|t_{SH}|)^2} \left(\frac{\alpha_f{}^2 (1-|t_f|^2)}{(1-\alpha_f |t_f|)^2} \right)^2, \tag{63}$$

#149422 - $15.00 USD Received 20 Jun 2011; revised 25 Jul 2011; accepted 25 Jul 2011; published 15 Aug 2011

where $P_{SH}^{out} = \left|C_{1,SH}\right|^2$ and $P_f^{in} = \left|B_{1,f}\right|^2$. The parameters α_i and t_i can be written in terms of the quality factors using Eq. (19).

Table 1 compares the SH conversion efficiency calculated using coupled-mode theory Eq. (62), and η calculated using the generalized waveguide-microresonator theory Eq. (63). The GaAs microdisk has R = 2.609 μm and h = 161 nm, and supports doubly resonant SHG with $\lambda_f = 2\lambda_{SH}$ = 1998.7 nm with TE-polarized fundamental wave (m_f = 13) and TM-polarized SH wave (m_{SH} = 28) where $\Delta m = m_{SH} - 2m_f = 2$ is satisfied ($p_f = p_{SH} = q_f = q_{SH} = 1$). The free-spectral ranges for the waves are $\delta f_{FSR,f} = 6.3\times10^{12}$ Hz and $\delta f_{FSR,SH} = 3.4\times10^{12}$ Hz. We use d_{14} = 94 pm/V [31] for GaAs. CMT predicts a SH conversion efficiency of 1.23% while the GWMT predicts η = 1.16% for 1 mW of incident fundamental power. There is good agreement between the two theories.

Table 1. Comparison between coupled-mode theory (CMT), which utilizes the energy normalization and Eq. (62), and on-resonance generalized waveguide-microresonator theory (GWMT) discussed in Section 2, which utilizes the power normalization and Eq. (63). The incident fundamental power P_f^{in} = 1 mW.

	CMT	GWMT
Coupling parameter (λ_f)	$Q_f^c = 10^4$	$1-\left\|t_f\right\| = 7.4\times10^{-3}$
Loss parameter (λ_f)	$Q_f^0 = 10^4$	$1-\alpha_f = 7.4\times10^{-3}$
Coupling parameter (λ_{SH})	$Q_{SH}^c = 10^4$	$1-\left\|t_{SH}\right\| = 2.7\times10^{-2}$
Loss parameter (λ_{SH})	$Q_{SH}^0 = 10^4$	$1-\alpha_{SH} = 2.7\times10^{-2}$
K_+	$K_+^{en} = 3.32\times10^3\,(\mathrm{W\cdot s})^{-1/2}$	$K_+^{pow} = 9.66\times10^{-4}\ \mathrm{W}^{-1/2}$
K_-	$K_-^{en} = -6.67\times10^3\,(\mathrm{W\cdot s})^{-1/2}$	$K_-^{pow} = -1.94\times10^{-3}\ \mathrm{W}^{-1/2}$
$\eta = P_{SH}^{out} / P_f^{in}$	1.23 %	1.16 %

Acknowledgements

We thank Kartik Srinivasan for helpful discussions. P. S. Kuo acknowledges support from the National Research Council Postdoctoral Research Associate program. We also acknowledge support through the NSF Physics Frontier Center at the Joint Quantum Institute and the Zeno-based Optoelectronics program at DARPA.

#149422 - $15.00 USD Received 20 Jun 2011; revised 25 Jul 2011; accepted 25 Jul 2011; published 15 Aug 2011